

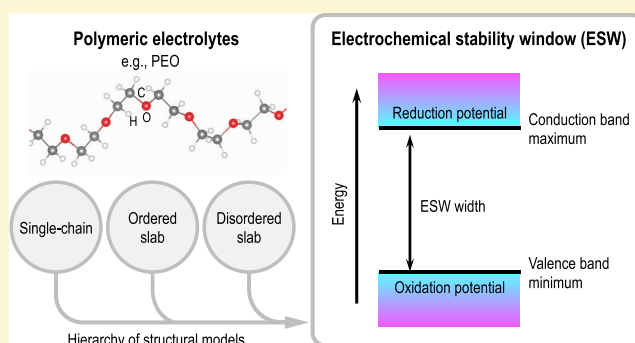
# Electrochemical Stability Window of Polymeric Electrolytes

Lihua Chen,<sup>1</sup> Shruti Venkatram, Chiho Kim,<sup>1</sup> Rohit Batra,<sup>1</sup> Anand Chandrasekaran, and Rampi Ramprasad<sup>1\*</sup>

School of Materials Science and Engineering, Georgia Institute of Technology, 771 Ferst Drive NW, Atlanta, Georgia 30332, United States

## Supporting Information

**ABSTRACT:** The electrochemical stability window (ESW) is a fundamental consideration for choosing polymers as solid electrolytes in lithium-ion batteries. Morphological and chemical aspects of the polymer matrix and its complex interactions with lithium salts make it difficult to estimate the ESW of the polymer electrolyte, either computationally or experimentally. In this work, we propose a practical computational procedure to estimate the ESW due to just one dominant factor, i.e., the polymer matrix, using first-principles density functional theory computations. Diverse model polymers (10) were investigated, namely, polyethylene, polyketone, poly(ethylene oxide), poly(propylene oxide), poly(vinyl alcohol), polycaprolactone, poly(methyl methacrylate), poly(ethyl acrylate), poly(vinyl chloride), and poly(vinylidene fluoride). For each case, an increasingly complex hierarchy of structural models was considered to elucidate the impact of polymer chemistry and the morphological complexity on the ESW. Favorable agreement between the computed ESW of disordered slabs and the corresponding experimental values provides confidence in the reliability of the computational procedure proposed in this work. Additionally, this study provides a baseline for subsequent systematic investigations of the impact of additional factors, such as the presence of lithium salts and electrode–electrolyte interfaces. The present work, thus, constitutes an important initial step toward the rational design of novel polymer electrolytes with desired ESW values.



## INTRODUCTION

Polymer electrolytes are safe and promising replacements for liquid electrolytes in Li-ion batteries given their superior electrochemical, mechanical, and thermal stability and easy processability.<sup>1–8</sup> Typically, polymer electrolytes consist of a polymer matrix (e.g., poly(ethylene oxide) (PEO) or poly(vinylidene fluoride) (PVDF)) and dissolved lithium salts (e.g., LiClO<sub>4</sub>, LiBF<sub>4</sub> or LiPF<sub>6</sub>). To be a suitable electrolyte, the host polymer should possess a set of properties, including large electrochemical stability window, low glass transition temperature, high ionic conductivity and Li-ion transference, etc., whereas the salts should have a lower melting point and good solubility in the host polymers. Given the chemical and morphological complexity of the polymer matrix, numerous possibilities of lithium salts and their complex physical and chemical interactions, the discovery of novel polymer electrolytes, which meet the aforementioned criteria, is very time and cost intensive via experimental methods.<sup>1–8</sup>

The electrochemical stability window (ESW) is a crucial consideration for polymer electrolytes, controlling its open circuit voltage ( $V_{oc}$ ) and, therefore, the cycle life of Li-ion batteries.<sup>1–8</sup> As shown in Figure 1, ESW of the electrolyte is determined by its reduction and oxidation potentials, which is governed by the conduction band maximum (CBM) and the valence band minimum (VBM), respectively.<sup>4,7,9,10</sup> For

utilization as an electrolyte, a polymer should have a large ESW width, i.e., the energy gap between CBM and VBM should exceed the energy difference of the electrochemical potentials of the anode ( $\mu_A$ ) and cathode ( $\mu_C$ ). Additionally,  $\mu_A$  and  $\mu_C$  should be within the energy gap of the polymer electrolyte, i.e., CBM >  $\mu_A$  and VBM <  $\mu_C$ . Failure to meet these requirements can lead to the formation of a passivation layer at the electrode/electrolyte interfaces. Although this layer can increase the electron-transfer barrier across the interface, it also blocks the transfer of Li<sup>+</sup> ions to the electrolyte, thereby, reducing the cycling life of the battery.

To quantify the ESW parameters (i.e., CBM, VBM, and ESW width), extensive experimental or computational efforts have been made. Experimentally, the ESW width of polymers can be measured using the optical absorption spectra<sup>11–18</sup> and cyclic voltammetry measurements.<sup>1–5,19–21</sup> However, these methods are very time consuming and provide little information about the positioning of the polymer band edges relative to the electrodes (as illustrated in Figure 1). Alternatively, first-principles density functional theory (DFT) has been widely used to study the ESW of ionic liquids

Received: April 18, 2019

Revised: May 25, 2019

Published: May 28, 2019

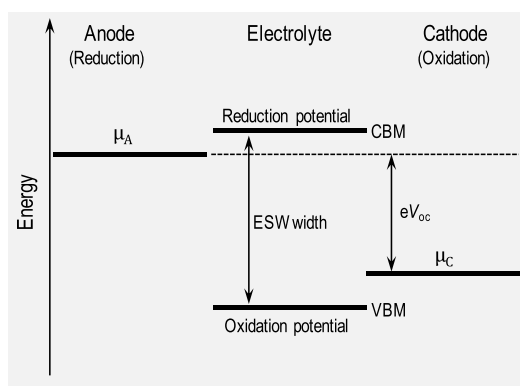


**Figure 1.** Energy diagram of the electrolyte interface with anode and cathode. ESW of the electrolyte is determined by its reduction and oxidation potentials, controlled by the conduction band maximum (CBM) and the valence band minimum (VBM), respectively.  $\mu_A$  and  $\mu_C$  are the electrochemical potentials of the anode and the cathode, respectively. The CBM and VBM difference is the ESW width and  $\mu_A - \mu_C = eV_{oc}$ , here,  $V_{oc}$  and  $e$  are the open circuit voltage and the electron charge, respectively.

electrolytes,<sup>4,7,9</sup> carbonate-based molecules,<sup>22</sup> and aprotic candidates.<sup>23</sup> To the best of our knowledge, the ESW of polymer electrolytes remain largely unexplored, even for the case of commonly used PEO electrolyte.<sup>10,24–27</sup> The main reasons being the intricate interplay of various factors affecting the ESW of polymer electrolytes, such as the complex chemical and morphological variations present in the polymer matrix, different interactions between the polymer electrolytes and the lithium salts, and limited knowledge of the nature of the electrode–electrolyte interfaces. Thus, determining the role of such factors on the ESW of polymer electrolytes is far from trivial.

In this contribution, we attempt to unravel the role of one of the most important factors, i.e., the polymer matrix, in determining the ESW of polymer electrolytes and establish a computational procedure to reliably estimate ESW parameters using high-throughput DFT computations and classical molecular dynamics (MD) simulations. As shown in Figure 2, 10 model polymers, including 8 common polymer matrices (i.e., PEO, PVDF, poly(propylene oxide) (PPO), polycaprolactone (PCL), poly(vinyl alcohol) (PVA), poly(methyl methacrylate) (PMMA), poly(ethyl acrylate) (PEA), and poly(vinyl chloride) (PVC)) and 2 polymers with simple polymer chemistry (i.e., polyethylene (PE) and polyketone (PK)), were investigated. To probe the effect of the polymer morphology, a hierarchy of models, i.e., the single-chain, ordered, and disordered slabs, with varying structural complexities were considered. Although the single-chain model represents the simplest case and is intended to capture the effect of monomer chemistry, the ordered and disordered slabs (generated via classical MD simulations) were used to represent the crystalline and the amorphous regions of a semicrystalline polymer, respectively. Collectively, these hierarchical models allow to clearly elucidate the role of chemistry and morphology in each polymer. A comparison of ESW parameters obtained from all three models against the available experimental values suggests that the disordered slab model, in general, provides the most accurate estimate with reasonably small errors. Thus, the proposed approach of using a combination of classical MD and DFT calculations is not only an efficient way to accurately predict the ESW of polymer electrolytes but also lays the groundwork for further studies on lithium salts and electrode–electrolyte interfaces.

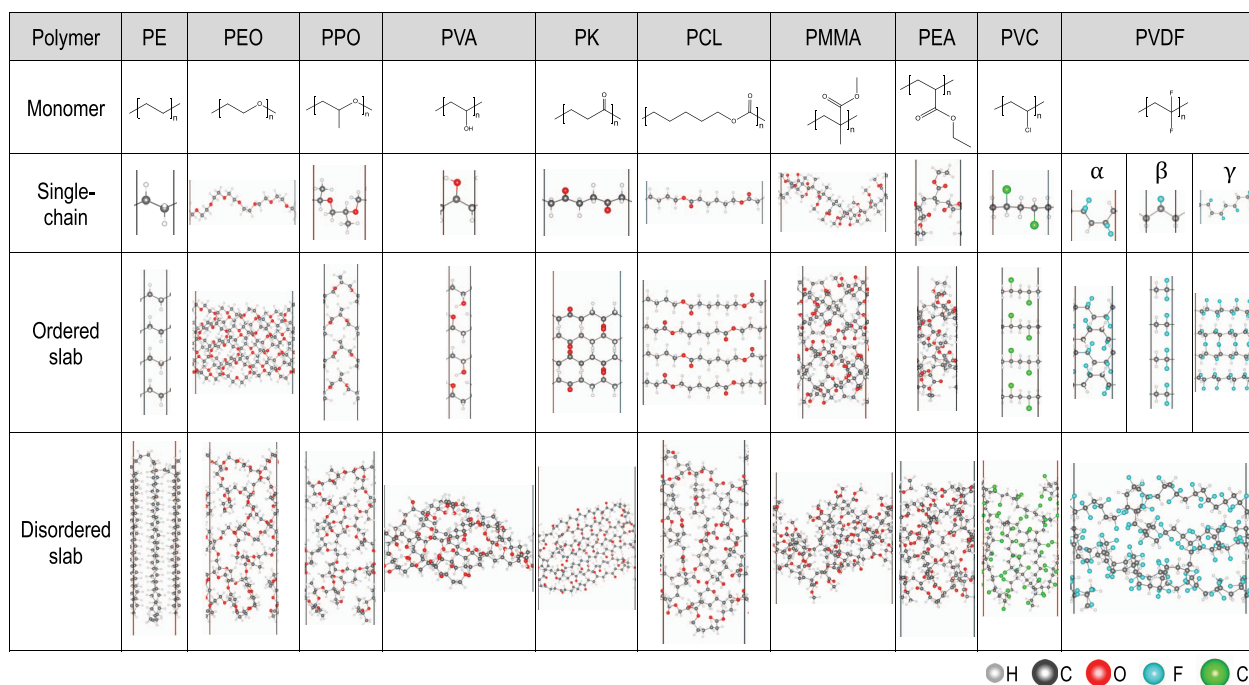


**Figure 2.** Physical structures of the single-chain, ordered, and disordered slabs of the 10 model polymers considered in this work. The C, H, O, Cl, F atoms are denoted by gray, white, red, green, and cyan spheres, respectively. For the case of ordered slabs, one of the two periodic orientation is not visible.

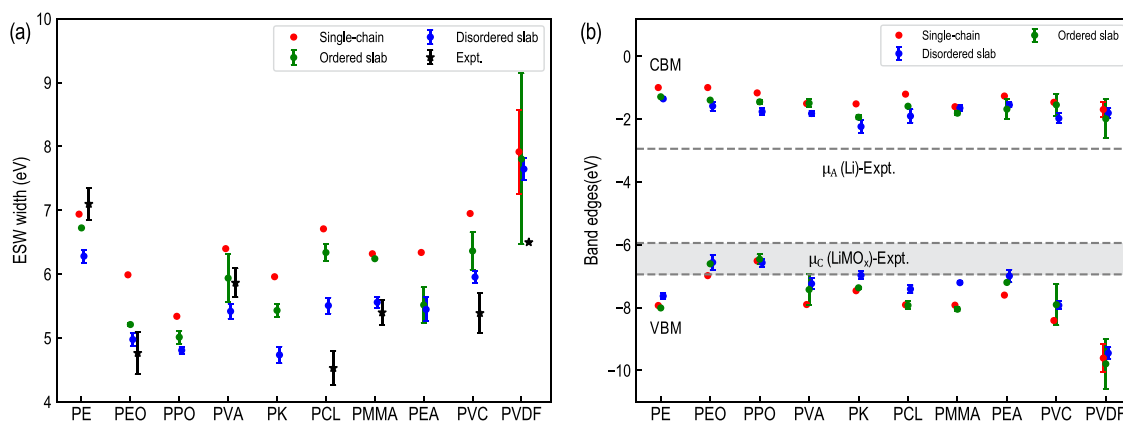


**Figure 3.** DFT-predicted ESW parameters: ESW width (a) and band edges (b) of the 10 model polymers. Error bars of ordered and disordered slabs are derived from slabs along two directions and five configurations considered, respectively. Available experimental values from the literature are also provided, shown as black stars. All energy levels in (b) are with respect to the vacuum energy (0 eV).  $\mu_A$  of the Li anode is determined by the energy difference between the vacuum energy and the experimental work function of Li,<sup>49</sup> whereas  $\mu_C$  of lithium transition-metal oxides ( $\text{LiMO}_x$ ,  $M = \text{Co, Mn, Fe, Ni, etc.}$ ) cathodes is the energy difference of  $\mu_A$  and  $eV_{\text{oc}}^{\text{expt.}}$  of  $\text{LiMO}_x$ .<sup>50,51</sup>

## MODELS AND COMPUTATIONAL DETAILS

**Models.** Figure 2 illustrates the three hierarchical models considered for the 10 model polymers. As the name suggests, the single-chain model consists of a periodic chain along one axis, with vacuum regions (14–15 Å) in the other two directions. Ordered slabs represent the crystalline regions of a semicrystalline polymer that were constructed based on DFT-relaxed crystal structures, details of which are provided in Table S1 of the Supporting Information (SI). The ordered slab models comprise of four polymer chains arranged such that there is periodicity along two directions (including the chain axis) and a vacuum region (around 15–16 Å) along the third axis. In this case, statistics was attained by considering both (100) and (010) slab orientations, with a representative example for each polymer shown in Figure 2. Further, with regards to tacticity, only cases with isotactic PVA, isotactic PMMA, isotactic PEA, and syndiotactic PVC were considered. For PVDF, three phases ( $\alpha$ ,  $\beta$ ,  $\gamma$ ) of crystal structures were used to construct the single-chain and ordered slabs. To study the amorphous regions of polymers, disordered slabs were generated via classical MD simulations of a supercell containing a single finite polymer chain, made up 30–50 repeat units with terminated H atoms. These chain lengths were kept significantly longer to include a variety of morphological disorders and to ascertain that no artificial error in the polymer electronic structure is introduced due to smaller chain lengths.<sup>28,29</sup>

**Computational Details.** *General Computational Scheme.* All DFT calculations were performed using the Vienna Ab initio Simulation Package (VASP),<sup>30</sup> with the projector-augmented wave method<sup>31</sup> and a plane-wave energy cutoff  $E_{\text{cut}}$  of 400 eV. The Perdew–Burke–Ernzerhof exchange–correlation (XC) functional<sup>31</sup> and the vdW-DF2 functional<sup>32–36</sup> were used to fully relax the single-chain and ordered slabs until atomic forces were less than 0.01 eV/Å. The adopted Monkhorst–Pack  $k$ -point meshes<sup>37</sup> for each system are summarized in Table S2 of the SI.

To generate the disordered slabs, classical MD simulations based on the OPLS-AA force field (for PE, PEO, PPO, PVA, PCL, PMMA, and PEA)<sup>38</sup> and the PCFF force field (for PK, PVC and PVDF)<sup>39</sup> were performed using the LAMMPS simulation package<sup>40</sup> with a time step of 1 fs. The details of the

adopted melt-quench procedure include: (1) a constant number (N)–volume (V)–temperature (T) (NVT) simulation at  $T = 600$  K for 1 ns on a single polymer chain; (2) cooling from 600 to 300 K using an NVT ensemble for 1 ns; (3) further equilibration at 300 K for 1 ns using NVT simulation; (4) 5 ns NPT simulations (here,  $P$  (pressure) = 1 atm,  $T = 300$  K). During the last NPT run, the MD trajectories from 4 to 5 ns were further examined using torsion angle autocorrelations function ( $R_\phi$ ) (Figure S1 of the SI) to confirm system equilibration. Five representative configurations with various  $R_\phi$  values were sampled from the last 0.5 ns for ESW calculations, with the sampling procedure discussed in the SI. Figure 2 shows an example of disordered slab for each polymer with periodic boundaries along two directions and a vacuum region along the third axis.

**Estimation of ESW.** The ESW of the 10 model polymers were predicted using DFT with hybrid XC functional (HSE06). Single-point HSE06 computations were performed on fully relaxed single-chains and ordered slabs, and the equilibrated disordered slabs directly obtained from MD simulations. Average values of five configurations for the disordered slabs and of (100) and (010) orientations for the ordered slab were used to estimate the CBM, VBM, and ESW width. For PVDF, the averaging was performed for all three different phases ( $\alpha$ ,  $\beta$ ,  $\gamma$ ) in the case of single-chain and ordered slab models. The CBM and VBM energy levels in Figure 3 are adjusted with respect to the vacuum level of each structure.

## RESULTS

**Physical Structures.** Figure 2 shows physical structures of the single-chain, ordered, and disordered slabs of the 10 model polymers. As mentioned earlier, the single chain is the least complex model incorporating only the monomer chemistry, while neglecting the interchain interactions and the intrachain morphological disorders within polymers. The interchain interactions are accounted in the ordered slabs, which contain multiple ordered packing chains along two nonbackbone directions. The ordered slabs for PEO, PPO, isotactic PMMA, and isotactic PEA chains follow 7/2, 3/1, 10/1 (double), 3/1 helical structures, respectively, which are known to be stable than their all-trans conformers. To model amorphous regions

**Table 1. DFT-Predicted ESW Parameters (CBM, VBM, Widths) of the 10 Model Polymers (given in eV), along with Experimental Results (Indirect Optical Band Gaps) for Pure Bulk Polymers**

polymers	single-chain			ordered slab			disordered slab			expt.
	VBM	CBM	width	VBM	CBM	width	VBM	CBM	width	width
PE	-7.93	-0.99	6.94	-8.01 ± 0.01	-1.28 ± 0.01	6.72 ± 0.01	-7.63 ± 0.09	-1.35 ± 0.04	6.28 ± 0.10	7.4 <sup>b</sup> , 6.9 <sup>c</sup>
PEO	-6.98	-0.99	5.99	-6.60 ± 0.01	-1.39 ± 0.01	5.21 ± 0.02	-6.55 ± 0.24	-1.58 ± 0.14	5.00 ± 0.10	4.43–5.10 <sup>d</sup>
PPO	-6.51	-1.16	5.34	-6.46 ± 0.16	-1.44 ± 0.06	5.01 ± 0.10	-6.57 ± 0.12	-1.76 ± 0.12	4.81 ± 0.06	
PVA	-7.90	-1.50	6.40	-7.42 ± 0.50	-1.49 ± 0.13	5.94 ± 0.37	-7.23 ± 0.17	-1.82 ± 0.09	5.42 ± 0.12	5.45–6.28 <sup>e</sup>
PK	-7.46	-1.51	5.90	-7.37 ± 0.04	-1.93 ± 0.07	5.43 ± 0.11	-6.97 ± 0.13	-2.23 ± 0.19	4.74 ± 0.13	
PCL	-7.91	-1.20	6.71	-7.93 ± 0.13	-1.59 ± 0.01	6.34 ± 0.14	-7.40 ± 0.12	-1.90 ± 0.21	5.51 ± 0.13	4.26 <sup>f</sup> , 4.8 <sup>e</sup>
PMMA	-7.92	-1.60	6.32	-8.05 ± 0.07	-1.81 ± 0.06	6.24 ± 0.01	-7.20 ± 0.04	-1.64 ± 0.10	5.56 ± 0.08	5.2, 5.6 <sup>g</sup>
PEA	-7.60	-1.26	6.34	-7.20 ± 0.03	-1.68 ± 0.31	5.52 ± 0.28	-6.99 ± 0.21	-1.54 ± 0.08	5.45 ± 0.19	
PVC	-8.41	-1.48	6.93	-7.90 ± 0.65	-1.54 ± 0.36	6.36 ± 0.29	-7.93 ± 0.13	-1.97 ± 0.15	5.96 ± 0.10	5.7 <sup>h</sup> , 5.08 <sup>i</sup>
PVDF <sup>a</sup>	-9.60	-1.69	7.91	-9.79 ± 0.79	-1.98 ± 0.63	7.80 ± 1.34	-9.44 ± 0.18	-1.80 ± 0.15	7.64 ± 0.16	6.5 <sup>j</sup>

<sup>a</sup>Average values of  $\alpha$ ,  $\beta$ ,  $\gamma$  phases of PVDF were used for the single-chain and ordered slabs. <sup>b</sup>Ref 12. <sup>c</sup>Ref 13. <sup>d</sup>Refs 11, 14, 41. <sup>e</sup>Ref 15, 42–44. <sup>f</sup>Ref 16. <sup>g</sup>Ref 45. <sup>h</sup>Ref 18. <sup>i</sup>Ref 46. <sup>j</sup>Refs 47, 48.

of polymers, disordered slabs were generated with various morphological disorders, as shown in Figure 2. These structures are validated using the torsion angle autocorrelations and radial distribution functions, as shown in Figures S1 and S2 of the SI, indicating that only representative equilibrated structures (bond lengths and torsion angles) were sampled.

**ESW Predictions.** Figure 3 and Table 1 summarize the DFT-predicted ESW of the single-chain, ordered, and disordered slabs of the 10 model polymers, together with available experimental values.<sup>11–16,41–48</sup> For the disordered slabs, the average and standard deviation values of five configurations considered are also included. Further, all energy levels in Figure 3(b) are reported with respect to the vacuum energy.

The single-chain model although not complex, reveals the role of monomer chemistry in the polymer ESW. For PE, the valence band edges are controlled by the  $sp^3$ -hybridized  $\sigma$  bonds, and the conduction band is due to the overlapping  $\sigma^*$  antibonding orbitals, resulting in a large ESW. For oxygen-containing polymers, i.e., PEO, PPO, PVA, PCL, PK, PMMA, and PEA, the valence band edges are controlled by nonbonding orbitals of O atoms (lone pairs electrons), resulting in close VBM values except for PEO and PPO (see Figure 3(b)). The higher VBM values of PEO and PPO are induced by their helical chain ordering in which the conformational disorder of C–O bonds greatly raises the  $\sigma_{C-O}$  bonding and nonbonding orbital energy levels. Additionally, the conduction band edges of PEO, PPO, and PVA are determined by the  $\sigma_{C-O}^*$  antibonding orbitals. However, the additional  $\sigma_{O-H}^*$  antibonding orbitals in PVA can degrade the  $\sigma_{C-O}^*$  energy levels, leading to a lower CBM compared to PEO and PPO. For PK, PCL, PMMA, and PEA, the  $\pi_{C=O}^*$  antibonding orbitals determine the conduction band edges. Although for PCL, PMMA, and PEA, the adjacent O atom in O=C–O groups can weaken the C=O bonding/antibonding energies, leading to the shift-down/up of the VBM/CBM resulting in higher ESW widths compared to PK.

For PVC and PVDF, the valence band edges are controlled by nonbonding orbitals of Cl and F atoms, respectively. The error bars for the case of single-chain PVDF in Figure 3 are a result of its three crystal phases. Depending on the electro-negativity, the nonbonding orbitals energies of O, Cl, and F follow the order: Cl < O < F, which explains PVDF's VBM, which is the lowest in comparison. However, due to the hybridization between the  $\pi_{C=O}$  bonding and the nonbonding

orbitals, PCL's VBM is higher than PVC's. PVC's and PVDF's CBM are determined by the  $\sigma_{C-Cl}^*$  and  $\sigma_{C-F}^*$  antibonding orbitals, respectively, the energies of which are lower than PCL's  $\pi_{C=O}^*$  antibonding orbitals. Because of the two  $\sigma_{C-F}^*$  bonds present in PVDF, its CBM is slightly lower than PVC's. However, the VBM values play a dominant role in determining the ESW, resulting in PVC's ESW < PVDF's ESW.

An important trend to note from Figure 3 is that the DFT-predicted ESW widths of the 10 model polymers generally follow the order: single-chain > ordered slabs > disordered slabs, indicating that interchain interactions and morphological disorders of polymers play a significant role in determining ESW. The ordered slab models include the interchain interactions, which can greatly degrade the overlap of antibonding orbitals between the polymer chains, leading to smaller ESW width. For example, in the ordered slabs of PEO, the formation of H-bonds between the O lone pair electrons and H atoms lead to a significant drop (0.4 eV) in the antibonding orbitals and, thus, a smaller ESW width. However, the ordered slab model has a practical limitation: the slab orientations can introduce net dipole moments (internal electric field), especially for polymers with side polar groups. As a result, an artificially smaller ESW width is obtained due to the shift-up of VBM and the shift-down of CBM. Moreover, the ESW of ordered slabs is sensitive to the slab orientations. Taking the ordered slab of PVA as an example, the net dipole moment induced by the (100)-ordered slabs is 20 times larger than that of the (010)-ordered slab. As a result, the ESW widths of the ordered (100) and (010) slabs are 5.56 and 6.31 eV, respectively. Similar observations are obtained for PEA, PVC, and PVDF. However, due to the presence of two highly polar C–F bonds in the PVDF monomer and consideration of its various crystal phases, the standard deviation in PVDF ESW width is up to 1.34 eV. On the other hand, for PEO-, PPO-, PCL-, and PMMA-ordered slab, the standard deviations in the ESW induced by slab orientations are less than 0.1 eV owing to their helical structure or presence of polar groups within the polymer backbone (or chain direction). The single-chain models can also suffer from the same problem, however, caution was exercised to ensure that polar groups were normal to the vacuum direction.

Nonetheless, the dipole moment artifact of the single-chain and ordered slab models can be addressed in the disordered slabs by inducing various isotropic conformational disorders, resulting in a net dipole moment which is close to zero.

Figure 3 shows the effect introduced by various conformational disorders in polymers due to significant distortions in the overlap of bonding and/or antibonding orbitals, resulting in the shift-up (down) of VBM (CBM) (blue circles in Figure 3(b)). Thus, disordered slabs have the lowest ESW width.

In general, the ESW widths of disordered slabs are closest to available experimental values (Figure 3(a)), as this structural model best represents the experimental situation. However, for PCL, PVC, and PVDF, the ESW widths are overestimated, which may be caused by structural deviations between the disordered models and experiments, the limited accuracy of classical force fields, and/or the artificial band gap problem introduced due to periodic boundary conditions while performing DFT computations. Another source could be the uncertainty in the experimental measurements due to additives or impurities.

## DISCUSSION AND OUTLOOK

From Figure 3 and Table 1, several conclusions can be made. First, details of the computed electronic structure of the disordered slabs come closest to the corresponding experimental results for the 10 model polymers. This is not surprising since the disordered slabs are structurally most similar to the real polymers. Therefore, we believe that the approach of using a combination of DFT calculations and classical MD simulations is a good practical method to predict the ESW of polymer electrolytes. However, the classical MD simulations are limited by the availability of reliable polymer force fields, which can perhaps be addressed by training force fields based on the data generated by this work (available on <https://khazana.gatech.edu/shorturl/esw>) using machine learning (ML) techniques.<sup>52–55</sup>

Second, our computational results show that all 10 model polymers are promising electrolyte candidates, with large ESW widths ( $>4.74$  eV). To further validate the VBM and CBM positions of 10 model polymers,  $\mu_A$  of the Li anode and  $\mu_C$  of lithium transition-metal oxides ( $\text{LiMO}_x$ ,  $M = \text{Co, Mn, Fe, Ni}$ , etc.) cathodes are also shown in Figure 3(b).  $\mu_A(\text{Li})$  was computed by the energy difference between the vacuum energy and the experimental work function of Li,<sup>49</sup> whereas  $\mu_C(\text{LiMO}_x)$  is determined by the energy difference of  $\mu_A(\text{Li})$  and  $eV_{\text{oc}}^{\text{expt.}}$  of  $\text{LiMO}_x$  ( $V_{\text{oc}}^{\text{expt.}}$ , 3–4 V, with respect to  $\text{Li}/\text{Li}^+$ ).<sup>50,51</sup> In general, the CBM and VBM values of the 10 model polymers fulfill the criteria for polymer electrolytes, i.e.,  $\text{CBM} > \mu_A$  and  $\text{VBM} > \mu_C$ .

Also, we find that the energy differences between the  $\mu_A(\text{Li})$  and CBM are slightly different for the 10 model polymers, whereas the energy difference between the  $\mu_C(\text{LiMO}_x)$  and VBM of disordered slabs follows the order,  $\text{PEO} \sim \text{PPO} < \text{PVA} \sim \text{PK} \sim \text{PCL} \sim \text{PMMA} \sim \text{PEA} < \text{PE} < \text{PVC} < \text{PVDF}$ . The latter reflects the ease of charge transfer between the cathode and the polymer electrolyte (i.e., chemical reactions), which can further be used to screen suitable polymer electrolytes. Moreover, the VBM of polar polymers in Figure 3 is determined by O/Cl/F lone pair electrons, which bond with the  $\text{Li}^+$  ions. Therefore, the trend in VBM of polar polymers can serve as a proxy for  $\text{Li}^+$  binding energies in these polymers. Lower VBM results in higher  $\text{Li}^+$  binding energies, assisting the dissociation of  $\text{Li}^+$  ions from original salts and accelerating the  $\text{Li}^+$  diffusion with the aid of segmental motions of polymers. These findings could be a reason why blend polymers of PEO-PMMA or PEO-P(VDF-TrFE) show much higher ionic conductivities than pure PEO polymers,<sup>6</sup> in

addition to an increase in amorphous regions in the former case.

Third, Figure 3 can serve as the starting point for investigating the impact of lithium salts and electrode–electrolyte interfaces on the ESW of polymer electrolytes. Past experimental work on PEO and PVA<sup>11,42</sup> indicates that doped lithium salts can decrease the ESW width of polymer electrolytes up to 1.5 eV, depending on the types and concentrations of lithium salts. Therefore, ESW widths of polymer electrolytes with different salts can be qualitatively obtained by subtracting 0.5–1.5 eV from the computed results in this work. However, little information is available about the effects of interactions between lithium salts and “real” polymers (with morphological disorders) on the reduction and oxidation (CBM and VBM) positions.<sup>10,25</sup> Moreover, the electrode–electrolyte interfaces can significantly degrade the CBM and VBM positions, due to charge transfer, chemical reactions, and electrolyte decomposition.<sup>4,8,56–58</sup> The proposed computational procedures and hierarchical models utilized in this work can provide useful and practical direction for such future studies.

Finally, we note that the computational procedure adopted in this work to predict the ESW of polymer electrolytes is, unfortunately, time intensive. Thus, there might be an opportunity to use a simple and inexpensive ML-based surrogate models to allow instant estimations of different ESW parameters, thereby, permitting screening of polymer electrolyte candidates from a much larger chemical space.<sup>55,59–63</sup> Some promise is already shown by Polymer Genome models (based on the Gaussian process regression and hierarchical fingerprinting scheme) that reasonably capture the ESW parameters of single-chain polymers.<sup>64–66</sup> Moving forward, these models can be improved in a multifidelity fashion,<sup>67</sup> wherein information from single-chain, ordered, and disordered slab models is simultaneously utilized to build ML models that aim to predict the ESW parameters closest to that of the real polymers. The hierarchical ESW data generated in this work can, thus, form the basis of such ML studies.

## SUMMARY

The electrochemical stability window (ESW) of the 10 model polymers, including PE, PEO, PPO, PVA, PK, PCL, PMMA, PEA, PVC, and PVDF, was estimated using high-throughput DFT calculations and classical MD simulations. A hierarchy of models with varying structural complexities, i.e., single-chain, ordered, and disordered slabs (generated by classical MD simulations), was considered to systematically study the effects of morphological disorders and polymer chemistry on the ESW and associated parameters (i.e., ESW width, VBM, and CBM). The key findings of this study include: (1) the morphological disorders in polymers can substantially distort the band edges, resulting in a decrease in ESW widths; (2) among the three hierarchical models considered, the ESW of disordered slab was found to be closest to the available experimental values, owing to its structural similarity with the real polymers; (3) all of the 10 polymers studied here were found to be promising electrolyte candidates with suitable ESW parameters.

The proposed computational procedure is a practical approach to predict the ESW of polymer electrolytes, which can be used to effectively screen and discover novel polymer electrolytes. This study lays the groundwork for further investigations of the impact of lithium salts and electrode–

electrolyte interfaces on ESW and other relevant properties (e.g., Li binding energies) for solid-state batteries.

## ■ ASSOCIATED CONTENT

### Supporting Information

The Supporting Information is available free of charge on the ACS Publications website at DOI: 10.1021/acs.chemmater.9b01553.

Geometric parameters of crystal structures of the 10 model polymers; physical structure characterization of disordered slabs: torsion angle autocorrelation function, radial distribution function; computational details: primary parameters in DFT calculations; sampling procedure of disordered slabs (PDF)

## ■ AUTHOR INFORMATION

### Corresponding Author

\*E-mail: rampi.ramprasad@mse.gatech.edu.

### ORCID

Lihua Chen: 0000-0002-9852-8211

Chiho Kim: 0000-0002-1814-4980

Rohit Batra: 0000-0002-1098-7035

Rampi Ramprasad: 0000-0003-4630-1565

### Notes

The authors declare no competing financial interest.

## ■ ACKNOWLEDGMENTS

This work is supported by the grant of “Kolon Center for Lifestyle Innovation” project. Computational support was provided by the Partnership for an Advanced Computing Environment (PACE) at the Georgia Institute of Technology, Atlanta, Georgia, United States and the Extreme Science and Engineering Discovery Environment (XSEDE).

## ■ REFERENCES

- (1) Sequeira, C.; Santos, D. *Polymer Electrolytes: Fundamentals and Applications*; Elsevier: Amsterdam, Netherlands, 2010.
- (2) Agrawal, R.; Pandey, G. Solid polymer electrolytes: materials designing and all-solid-state battery applications: an overview. *J. Phys. D: Appl. Phys.* **2008**, *41*, No. 223001.
- (3) Mindemark, J.; Sun, B.; Törmä, E.; Brandell, D. High-performance solid polymer electrolytes for lithium batteries operational at ambient temperature. *J. Power Sources* **2015**, *298*, 166–170.
- (4) Bhatt, M. D.; O'Dwyer, C. Recent progress in theoretical and computational investigations of Li-ion battery materials and electrolytes. *Phys. Chem. Chem. Phys.* **2015**, *17*, 4799–4844.
- (5) Stephan, A. M.; Nahm, K. Review on composite polymer electrolytes for lithium batteries. *Polymer* **2006**, *47*, S952–S964.
- (6) Long, L.; Wang, S.; Xiao, M.; Meng, Y. Polymer electrolytes for lithium polymer batteries. *J. Mater. Chem. A* **2016**, *4*, 10038–10069.
- (7) Goodenough, J. B.; Park, K.-S. The Li-ion rechargeable battery: a perspective. *J. Am. Chem. Soc.* **2013**, *135*, 1167–1176.
- (8) Xu, K. Electrolytes and Interphases in Li-Ion Batteries and Beyond. *Chem. Rev.* **2014**, *114*, 11503–11618.
- (9) Ong, S. P.; Andreussi, O.; Wu, Y.; Marzari, N.; Ceder, G. Electrochemical windows of room-temperature ionic liquids from molecular dynamics and density functional theory calculations. *Chem. Mater.* **2011**, *23*, 2979–2986.
- (10) Pandian, S.; Adiga, S.; Tagade, P.; Hariharan, K.; Mayya, K.; Lee, Y.-G. Electrochemical stability of ether based salt-in-polymer based electrolytes: Computational investigation of the effect of substitution and the type of salt. *J. Power Sources* **2018**, *393*, 204–210.
- (11) Chapi, S.; Raghu, S.; Subramanya, K.; Archana, K.; Mini, V.; Devendrapa, H. In *Conductivity and Optical Band Gaps of Polyethylene Oxide Doped with Li<sub>2</sub>SO<sub>4</sub> Salt*, AIP Conference Proceedings, 2014; pp 1275–1277.
- (12) Less, K. J.; Wilson, E. G. Intrinsic photoconduction and photoemission in polyethylene. *J. Phys. C: Solid State Phys.* **1973**, *6*, 3110.
- (13) Ohki, Y.; Fuse, N.; Arai, T. In *Band Gap Energies and Localized States in Several Insulating Polymers Estimated by Optical Measurements*, IEEE Conference on Electrical Insulation and Dielectric Phenomena (CEIDP), 2010; pp 1–4.
- (14) Mohan, V.; Bhargav, P.; Raja, V.; Sharma, A.; Narasimha Rao, V. Optical and electrical properties of pure and doped PEO polymer electrolyte films. *Soft Mater.* **2007**, *5*, 33–46.
- (15) Devi, C. U.; Sharma, A.; Rao, V. N. Electrical and optical properties of pure and silver nitrate-doped polyvinyl alcohol films. *Mater. Lett.* **2002**, *56*, 167–174.
- (16) Abdelrazek, E.; Hezma, A.; El-khodary, A.; Elzayat, A. Spectroscopic studies and thermal properties of PCL/PMMA biopolymer blend. *Egypt. J. Basic Appl. Sci.* **2016**, *3*, 10–15.
- (17) Yousif, E.; Abdallah, M.; Hashim, H.; Salih, N.; Salimon, J.; Abdullah, B. M.; Win, Y.-F. Optical properties of pure and modified poly (vinyl chloride). *Int. J. Ind. Chem.* **2013**, *4*, 4.
- (18) Ameer, A. A.; Abdallah, M. S.; Ahmed, A. A.; Yousif, E. A. Synthesis and characterization of polyvinyl chloride chemically modified by amines. *Open J. Polym. Chem.* **2013**, *3*, 11.
- (19) Judez, X.; Zhang, H.; Li, C.; Gonzalez-Marcos, J.; Zhou, Z.; Armand, M.; Rodriguez-Martinez, L. M. Lithium Bis(fluorosulfonyl)-imide/Poly(ethylene oxide) Polymer Electrolyte for All Solid-State Li-S Cell. *J. Phys. Chem. Lett.* **2017**, *8*, 1956–1960.
- (20) Arya, A.; Sharma, A. Insights into the use of polyethylene oxide in energy storage/conversion devices: a critical review. *J. Phys. D: Appl. Phys.* **2017**, *50*, No. 443002.
- (21) Li, Q.; Chen, J.; Fan, L.; Kong, X.; Lu, Y. Progress in electrolytes for rechargeable Li-based batteries and beyond. *Green Energy Environm.* **2016**, *1*, 18–42.
- (22) Halls, M. D.; Tasaki, K. High-throughput quantum chemistry and virtual screening for lithium ion battery electrolyte additives. *J. Power Sources* **2010**, *195*, 1472–1478.
- (23) Korth, M. Large-scale virtual high-throughput screening for the identification of new battery electrolyte solvents: evaluation of electronic structure theory methods. *Phys. Chem. Chem. Phys.* **2014**, *16*, 7919–7926.
- (24) Gadjourova, Z.; Martín y Marero, D.; Andersen, K. H.; Andreev, Y. G.; Bruce, P. G. Structures of the Polymer Electrolyte Complexes PEO<sub>6</sub>:LiXF<sub>6</sub> (X = P, Sb), Determined from Neutron Powder Diffraction Data. *Chem. Mater.* **2001**, *13*, 1282–1285.
- (25) Das, D.; Chandrasekaran, A.; Venkatram, S.; Ramprasad, R. Effect of Crystallinity on Li Adsorption in Polyethylene Oxide. *Chem. Mater.* **2018**, *30*, 8804–8810.
- (26) Johansson, P.; Tegenfeldt, J.; Lindgren, J. Modelling lithium ion transport in helical PEO by ab initio calculations. *Polymer* **2001**, *42*, 6573–6577.
- (27) Borodin, O.; Olguin, M.; Ganesh, P.; Kent, P. R. C.; Allen, J. L.; Henderson, W. A. Competitive lithium solvation of linear and cyclic carbonates from quantum chemistry. *Phys. Chem. Chem. Phys.* **2016**, *18*, 164–175.
- (28) Chen, L.; Batra, R.; Ranganathan, R.; Sotzing, G.; Cao, Y.; Ramprasad, R. Electronic Structure of Polymer Dielectrics: The Role of Chemical and Morphological Complexity. *Chem. Mater.* **2018**, *30*, 7699–7706.
- (29) Chen, L.; Huan, T. D.; Ramprasad, R. Electronic Structure of Polyethylene: Role of Chemical, Morphological and Interfacial Complexity. *Sci. Rep.* **2017**, *7*, No. 6128.
- (30) Kresse, G.; Furthmüller, J. Efficient iterative schemes for ab initio total-energy calculations using a plane-wave basis set. *Phys. Rev. B* **1996**, *54*, 11169.
- (31) Perdew, J. P.; Burke, K.; Ernzerhof, M. Generalized gradient approximation made simple. *Phys. Rev. Lett.* **1996**, *77*, 3865.

- (32) Liu, C.-S.; Pilania, G.; Wang, C.; Ramprasad, R. How Critical Are the van der Waals Interactions in Polymer Crystals? *J. Phys. Chem. A* **2012**, *116*, 9347–9352.
- (33) Pham, T. H.; Ramprasad, R.; Nguyen, H.-V. Density-functional description of polymer crystals: A comparative study of recent van der Waals functionals. *J. Chem. Phys.* **2016**, *144*, No. 214905.
- (34) Dion, M.; Rydberg, H.; Schröder, E.; Langreth, D. C.; Lundqvist, B. I. Van der Waals Density Functional for General Geometries. *Phys. Rev. Lett.* **2004**, *92*, No. 246401.
- (35) Román-Pérez, G.; Soler, J. M. Efficient Implementation of a van der Waals Density Functional: Application to Double-Wall Carbon Nanotubes. *Phys. Rev. Lett.* **2009**, *103*, No. 096102.
- (36) Klimeš, J.; Bowler, D. R.; Michaelides, A. Van der Waals density functionals applied to solids. *Phys. Rev. B* **2011**, *83*, No. 195131.
- (37) Monkhorst, H. J.; Pack, J. D. Special points for Brillouin-zone integrations. *Phys. Rev. B* **1976**, *13*, 5188.
- (38) Robertson, M. J.; Tirado-Rives, J.; Jorgensen, W. L. Improved Peptide and Protein Torsional Energetics with the OPLS-AA Force Field. *J. Chem. Theory Comput.* **2015**, *11*, 3499–3509.
- (39) Sun, H.; Mumby, S. J.; Maple, J. R.; Hagler, A. T. An ab Initio CFF93 All-Atom Force Field for Polycarbonates. *J. Am. Chem. Soc.* **1994**, *116*, 2978–2987.
- (40) Plimpton, S. Fast Parallel Algorithms for Short-Range Molecular Dynamics. *J. Comput. Phys.* **1995**, *117*, 1–19.
- (41) Sasikala, U.; Kumar, P. N.; Rao, V.; Sharma, A. Structural, electrical and parametric studies of a PEO based polymer electrolyte for battery applications. *Int. J. Eng. Sci. Adv. Technol.* **2012**, *2*, 722–730.
- (42) Ahmad, H. M.; Sabeeh, S. H.; Hussien, S. A. Electrical and optical properties of PVA/LiI polymer electrolyte films. *Asian Trans. Sci. Technol.* **2012**, *1*, 16–20.
- (43) Abdallah, M.; Hamood, O.; Yousif, E. Study the Optical properties of Poly (vinyl alcohol) Doped Copper Chloride. *J. Al-Nahrain University* **2013**, *16*, 17–20.
- (44) Abdullah, O. G.; Aziz, S. B.; Omer, K. M.; Salih, Y. M. Reducing the optical band gap of polyvinyl alcohol (PVA) based nanocomposite. *J. Mater. Sci.: Mater. Electron.* **2015**, *26*, 5303–5309.
- (45) Al-Kadhemy, M. F. H.; Saeed, A. A.; Khaleel, R. I.; Al-Nuaimi, F. J. K. Effect of gamma ray on optical characteristics of (PMMA/PS) polymer blends. *J. Theor. Appl. Phys.* **2017**, *11*, 201–207.
- (46) El Sayed, A.; El-Sayed, S.; Morsi, W.; Mahrous, S.; Hassen, A. Synthesis, characterization, optical, and dielectric properties of polyvinyl chloride/cadmium oxide nanocomposite films. *Polym. Compos.* **2014**, *35*, 1842–1851.
- (47) Lopez-Encarnacion, J. M.; Burton, J.; Tsymbal, E. Y.; Velev, J. P. Organic multiferroic tunnel junctions with ferroelectric poly (vinylidene fluoride) barriers. *Nano Lett.* **2011**, *11*, 599–603.
- (48) Choi, J.; Dowben, P. A.; Pebley, S.; Bune, A.; Ducharme, S.; Fridkin, V.; Palto, S.; Petukhova, N. Changes in metallicity and electronic structure across the surface ferroelectric transition of ultrathin crystalline poly (vinylidene fluoride-trifluoroethylene) copolymers. *Phys. Rev. Lett.* **1998**, *80*, 1328.
- (49) Haynes, W. M. *CRC Handbook of Chemistry and Physics*; CRC Press, 2014.
- (50) Liu, C.; Neale, Z. G.; Cao, G. Understanding electrochemical potentials of cathode materials in rechargeable batteries. *Mater. Today* **2016**, *19*, 109–123.
- (51) Nitta, N.; Wu, F.; Lee, J. T.; Yushin, G. Li-ion battery materials: present and future. *Mater. Today* **2015**, *18*, 252–264.
- (52) Huan, T. D.; Batra, R.; Chapman, J.; Krishnan, S.; Chen, L.; Ramprasad, R. A universal strategy for the creation of machine learning-based atomistic force fields. *npj Comput. Mater.* **2017**, *3*, No. 37.
- (53) Botu, V.; Batra, R.; Chapman, J.; Ramprasad, R. Machine learning force fields: construction, validation, and outlook. *J. Phys. Chem. C* **2017**, *121*, 511–522.
- (54) Botu, V.; Ramprasad, R. Learning scheme to predict atomic forces and accelerate materials simulations. *Phys. Rev. B* **2015**, *92*, No. 094306.
- (55) Ramprasad, R.; Batra, R.; Pilania, G.; Mannodi-Kanakkithodi, A.; Kim, C. Machine learning in materials informatics: recent applications and prospects. *npj Comput. Mater.* **2017**, *3*, No. 54.
- (56) Butler, K. T.; Gautam, G. S.; Canepa, P. Designing interfaces in energy materials applications with first-principles calculations. *npj Comput. Mater.* **2019**, *5*, No. 19.
- (57) Wang, A.; Kadam, S.; Li, H.; Shi, S.; Qi, Y. Review on modeling of the anode solid electrolyte interphase (SEI) for lithium-ion batteries. *npj Comput. Mater.* **2018**, *4*, No. 15.
- (58) Gauthier, M.; Carney, T. J.; Grimaud, A.; Giordano, L.; Pour, N.; Chang, H.-H.; Fenning, D. P.; Lux, S. F.; Paschos, O.; Bauer, C.; et al. Electrode-electrolyte interface in Li-ion batteries: Current understanding and new insights. *J. Phys. Chem. Lett.* **2015**, *6*, 4653–4672.
- (59) Mannodi-Kanakkithodi, A.; Treich, G. M.; Huan, T. D.; Ma, R.; Tefferi, M.; Cao, Y.; Sotzing, G. A.; Ramprasad, R. Rational Co-Design of Polymer Dielectrics for Energy Storage. *Adv. Mater.* **2016**, *28*, 6277–6291.
- (60) Ma, R.; Sharma, V.; Baldwin, A. F.; Tefferi, M.; Offenbach, I.; Cakmak, M.; Weiss, R.; Cao, Y.; Ramprasad, R.; Sotzing, G. A. Rational design and synthesis of polythioureas as capacitor dielectrics. *J. Mater. Chem. A* **2015**, *3*, 14845–14852.
- (61) Baldwin, A. F.; Huan, T. D.; Ma, R.; Mannodi-Kanakkithodi, A.; Tefferi, M.; Katz, N.; Cao, Y.; Ramprasad, R.; Sotzing, G. A. Rational design of organotin polyesters. *Macromolecules* **2015**, *48*, 2422–2428.
- (62) Huan, T. D.; Mannodi-Kanakkithodi, A.; Kim, C.; Sharma, V.; Pilania, G.; Ramprasad, R. A polymer dataset for accelerated property prediction and design. *Sci. Data* **2016**, *3*, No. 160012.
- (63) Lorenzini, R. G.; Kline, W.; Wang, C.; Ramprasad, R.; Sotzing, G. The rational design of polyurea & polyurethane dielectric materials. *Polymer* **2013**, *54*, 3529–3533.
- (64) Kim, C.; Chandrasekaran, A.; Huan, T. D.; Das, D.; Ramprasad, R. Polymer Genome: A Data-Powered Polymer Informatics Platform for Property Predictions. *J. Phys. Chem. C* **2018**, *122*, 17575–17585.
- (65) Mannodi-Kanakkithodi, A.; Chandrasekaran, A.; Kim, C.; Huan, T. D.; Pilania, G.; Botu, V.; Ramprasad, R. Scoping the polymer genome: A roadmap for rational polymer dielectrics design and beyond. *Mater. Today* **2018**, *21*, 785–796.
- (66) Huan, T. D.; Mannodi-Kanakkithodi, A.; Kim, C.; Sharma, V.; Pilania, G.; Ramprasad, R. A polymer dataset for accelerated property prediction and design. *Sci. Data* **2016**, *3*, No. 160012.
- (67) Batra, R.; Ghanshyam, P.; Blas, U.; Rampi, R. Multi-fidelity information fusion with machine learning: A case study of dopant formation energies in hafnia. *ACS Appl. Mater. Interfaces* **2019**, DOI: 10.1021/acsami.9b02174.